nanomaterials

MDPI

Article

Microorganism-Templated Nanoarchitectonics of Hollow TiO_2-SiO_2 Microspheres with Enhanced Photocatalytic Activity for Degradation of Methyl Orange

Shenglan Liao [1,2], Liqin Lin [2,*], Jiale Huang [1], Xiaolian Jing [2], Shiping Chen [2] and Qingbiao Li [1]

[1] Department of Chemical and Biochemical Engineering, College of Chemistry and Chemical Engineering, Xiamen University, Xiamen 361005, China; shenglanliao@outlook.com (S.L.); cola@xmu.edu.cn (J.H.); kelqb@xmu.edu.cn (Q.L.)

[2] Department of Chemical Engineering and Pharmacy, College of Chemical Engineering and Materials Science, Quanzhou Normal University, Quanzhou 362000, China; jingxiaolian@foxmail.com (X.J.); shiping22@163.com (S.C.)

* Correspondence: liqin-100@163.com

Abstract: In this study, hollow SiO_2 microspheres were synthesized by the hydrolysis of tetraethyl orthosilicate (TEOS) according to the Stober process, in which *Pichia pastoris* GS 115 cells were served as biological templates. The influence of the preprocessing method, the TEOS concentration, the ratio of water to ethanol, and the aging time on the morphology of microspheres was investigated and the optimal conditions were identified. Based on this, TiO_2-SiO_2 microspheres were prepared by the hydrothermal process. The structures and physicochemical properties of TiO_2-SiO_2 photocatalysts were systematically characterized and discussed. The photocatalytic activity for the degradation of methyl orange (MO) at room temperature under Xe arc lamp acting as simulated sunlight was explored. The result showed that the as-prepared TiO_2-SiO_2 microspheres exhibited a good photocatalytic performance.

Keywords: hollow SiO_2 microspheres; biotemplate; TiO_2-SiO_2; photocatalyst

Citation: Liao, S.; Lin, L.; Huang, J.; Jing, X.; Chen, S.; Li, Q. Microorganism-Templated Nanoarchitectonics of Hollow TiO_2-SiO_2 Microspheres with Enhanced Photocatalytic Activity for Degradation of Methyl Orange. *Nanomaterials* **2022**, *12*, 1606. https://doi.org/10.3390/nano12091606

Academic Editors: Katsuhiko Ariga, Fabien Grasset and Yann Molard

Received: 5 April 2022
Accepted: 4 May 2022
Published: 9 May 2022

1. Introduction

The rapid development of the textile industry not only brings considerable economic benefits, but also aggravates environmental pollution. Due to the complex composition of textile wastewater and its high content of organic substances, harmful substances, and deep chroma, which cause serious harm to water bodies, the treatment of textile wastewater is imperative [1,2]. Water-soluble azo dyes including MO are the main targets of pollution control. Many treatment methods of dye removal have been investigated, including adsorption [3,4], photo-Fenton oxidation [5–7], H_2O_2/UV (ultraviolet) treatment [8,9], photocatalysis [10,11], and biological treatment [12–14]. Among these methods, photocatalysis is considered an effective method to degrade dyes in wastewater [15].

TiO_2 is considered to be one of the most promising photocatalysts for the removal of organic pollutants in textile wastewater due to its low cost, strong oxidizing properties, non-toxicity, and biochemical inertness [16–18]. However, there are some imperfections, such as its large energy gap, high photoelectric hole recombination rate, etc. [19–22]. The small nanoparticles have a high surface energy and readily form agglomerates, and their wide band gap (3.2 eV) makes them inactive under visible light irradiation. Moreover, the application in high temperature and high-pressure reactions is limited due to the poor mechanical strength and thermal stability of TiO_2. Therefore, researchers are looking for more effective methods with which to improve the surface-active sites of TiO_2, the photoelectron-hole separation rate, the solar energy usage efficiency, and the spectral response to enhance its photocatalytic performance [23]. One of the most promising

methods to enhance the activity of TiO_2 under visible light and sunlight irradiation is to dope non-metals such as N, C, and Si. Due to the difference in properties between Si and Ti, mesoporous SiO_2 is more stable than mesoporous TiO_2. Mesoporous TiO_2 can easily cause the collapse of the mesoporous structure when the template is removed by calcination at high temperatures, while silicon-based materials have a good thermal stability. Taking advantage of the good thermal stability of silicon-based materials, titanium-silicon composites could be prepared by loading titanium onto mesoporous silicon-based materials, which can effectively solve the pore structure instability of mesoporous TiO_2 [20].

The methods used for combining TiO_2 and SiO_2 can be roughly divided into two categories. One involves the mechanical mixture of TiO_2 and SiO_2. The other involves the use of chemical methods such as co-precipitation and sol–gel, where the composite oxide TiO_2-SiO_2 with Ti-O-Si bonds is obtained [24–26]. It is generally believed that TiO_2-SiO_2 oxides with Ti-O-Si bonds perform better as catalyst supports than mechanically mixed TiO_2-SiO_2 [27]. Among various composite oxides, TiO_2-SiO_2 composite oxides, especially in the mesoporous structure, exhibit a good chemical stability, availability, reusability, and controllability of pore structure [28]. Compared with other chemical methods, hydrothermal methods are often applied for the preparation of metal oxide materials because of their characteristics of a fast reaction speed, an adjustable structure, and crystallinity. In this study, microorganism cells-templated TiO_2-SiO_2 hollow microspheres were synthesized by the combination of the Stober process and the hydrothermal process and the photocatalytic activity for the degradation of methyl orange was investigated (see Figure A1).

2. Materials and Methods

2.1. Materials

TEOS (tetraethyl orthosilicate, purity $\geq$ 98%), TBOT (titanium butoxide, purity $\geq$ 99%), 25% ammonia solution (purity $\geq$ 99.5%), nitric acid (65.0~68.0%), methyl orange, and ethanol (purity $\geq$ 99.7%) were used without further purification. *Pichia pastoris* GS115 (*P. pastoris* GS115) cells were cultured in our laboratory.

2.2. Methods

2.2.1. Preparation of Hollow SiO_2 Microspheres

Hollow SiO_2 microspheres were synthesized using microorganism cells as templates according to the Stober process. In a typical experiment, 0.2 g of *P. pastoris* GS115 cells were suspended in 4.2 mL of ultrapure water and 10.5 mL of absolute ethanol (the ratio of water–ethanol was 1/2). The mixture was placed on a magnetic stirrer to stir at 25 °C for 1 h. Then, 6.4 mL of TEOS (1.2 mol/L, if not specified) was added and allowed to react for 2 h, followed by 2.85 mL of ammonia for another 1 h. The suspension was agitated at 25 °C for 12 h (if not specified). The product was separated by centrifugation (3500 r/min, 10 mins) and washed with ethanol and water several times. The precipitate was dried and calcinated at 550 °C for 2 h with a heating rate of 2 °C/min.

2.2.2. Preparation of TiO_2-SiO_2

A total of 2 g of the as-synthesized hollow SiO_2 microspheres was dispersed in 25 mL of anhydrous ethanol and 0.25 mL of TBOT. The solution was labeled as solution A. Then, 0.2 mL of nitric acid was added into the mixture of anhydrous ethanol (25 mL) and ultrapure water (10 mL). The solution was labeled as solution B. Solution A was continuously stirred at 25 °C for 5 min, and then solution B was added drop by drop and stirred for another 2 h. The mixture was transferred to a reaction kettle and heated at 180 °C for 24 h. After the hydrothermal reaction was completed, the samples were separated by centrifugation (3500 r/min, 10 min) and washed alternately with water and ethanol several times. The obtained samples were dried in an oven at 80 °C for 10 h and calcinated at 550 °C for 1 h with a heating rate of 2 °C/min.

2.2.3. Determination of Photocatalytic Performance

The photocatalytic experiments were carried out in a glass vessel by a 300 W Xe arc lamp acting as simulated sunlight. The initial concentration of the methyl orange was 10 mg/L. A total of 80 mg of the photocatalyst was taken in 80 mL of MO solution. Illumination was implemented after dark treatment for 1 h to reach adsorption–desorption equilibrium. At specific time intervals (every 20 min), 4 mL of the sample was taken from the suspensions and centrifuged to remove the catalyst prior to spectral measurement.

2.3. Characterization Methods

The crystal structure of the samples was determined by an X-ray diffractometer (XRD, X'Pert Pro MPD, Panalytical, The Netherlands) operated at a voltage of 40 kV and a current of 30 mA with Cu Kα radiation. The observations of morphology and microstructure were performed on a scanning electron microscope (SEM, ZEISS Sigma, Oberkochen, Germany) and a transmission electron microscope (TEM, Philips Tecnai F30, Eindhoven, The Netherlands) operated at an accelerating voltage of 300 kV. The specific surface area, pore volume, and pore size distribution of the samples were determined by Tristar-type low-temperature N_2 physical adsorption and desorption (BET, NOVA2200e, Quantachrome, Boynton Beach, FL, USA). The thermogravimetric (TG) studies were carried out on Netzsch TG209F1 thermobalance (NETZSCH Scientific Instruments Co., Selb, Germany) under a flowing-air atmosphere at a heating rate of 10 °C/min. X-ray Photoelectron Spectroscopy (XPS) measurements were performed on a PHI 5000 versa probe-II microprobe (Ulvac-Phi, Kanagawa, Japan). The UV-DRS analysis was performed on a UV-VIS Cary 5000 instrument (Varian, Palo Alto, CA, USA). $BaSO_4$ was served as a reference. The Fourier Transform Infrared Spectroscopy (FTIR) analysis was carried out on a Nicolet 6700 instrument (Thermo Fisher Scientific, Waltham, MA, USA).

3. Results and Discussion

3.1. Preparation of Hollow SiO_2 Microspheres

In recent years, inorganic hollow micro/nanostructures have attracted extensive attention due to their unique morphologies, unique physicochemical properties, and potential applications in dyes, drug delivery, and efficient catalysis [29,30]. The template method is one of the most commonly used methods for the synthesis of hollow nanomaterials [31]. The application of microorganisms as a template is considered to be an economical and green method [32–35]. Herein, the hollow SiO_2 was prepared by using the *P. pastoris* GS115 cells as a template and the influence of different reaction conditions on the structure were investigated.

3.1.1. Effect of Preprocessing Methods

Templates are vital for the preparation of hollow material. As shown in Figure 1a, solid SiO_2 microspheres with a particle size of 200–300 nm were obtained when no template was introduced. When *P. pastoris* GS 115 cells with the size of 1–2 μm were introduced, the obtained microspheres had successfully replicated the template structure (Figure 1b–d). The solvent has an obvious influence on the morphology. When *P. pastoris* GS 115 cells were suspended in ethanol or a hybrid system of ethanol and ammonia, there were many nano SiO_2 particles on the surface of hollow SiO_2, making the surface more rough and still agglomerate, which was shown in Figure 1b,c. While hollow, SiO_2 with a smooth surface and a good dispersion could be prepared if *P. pastoris* GS115 cells were firstly suspended in a water–ethanol mixture (the ratio of water–ethanol is 1/2, Figure 1d).

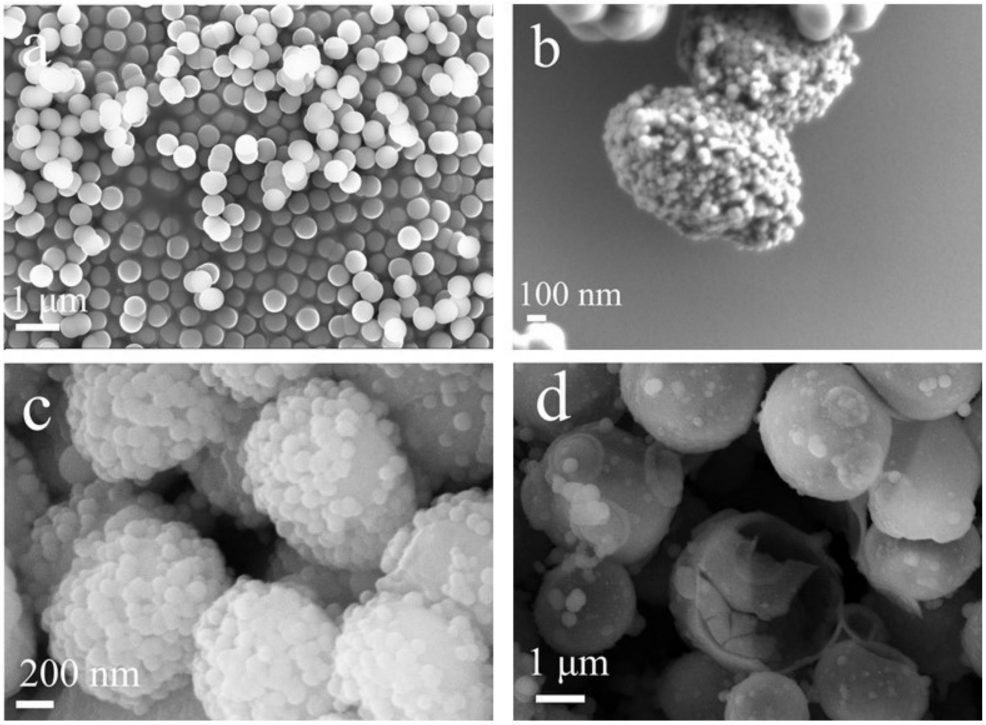

Figure 1. SEM images of SiO_2 prepared by different preprocessing methods: (**a**) without adding template; (**b**) *P. pastoris* GS 115 were suspended in ethanol and followed by TEOS and ammonia; (**c**) *P. pastoris* GS 115 were suspended in a hybrid system of ethanol and ammonia and followed by TEOS and ammonia; (**d**) *P. pastoris* GS 115 were suspended in an ethanol–water mixture and followed by TEOS and ammonia.

3.1.2. Effect of TEOS Concentration

The concentration of TEOS has an effect on the morphology of microspheres. When the TEOS concentration was low, small SiO_2 particles agglomerated and the concentration was not enough to form the complete hollow structure, as shown in Figure 2a. As the TEOS concentration gradually increased, more complete microspheres with hollow structure could successfully be prepared (Figure 2b–d). As the concentration of TEOS continued to increase, the excess SiO_2 particles continued to grow on the surface of the hollow SiO_2 microspheres due to the limited amount of templates. The surface of the prepared microspheres was relatively rough and agglomerated together to form larger clusters (Figure 2e). Therefore, to prepare hollow SiO_2 microspheres with a smooth surface and good dispersibility, the optimal TEOS concentration is between 1.0 and 1.2 mol/L.

3.1.3. Effect of the Ratio of Water to Ethanol

As shown in Figure 3, when the ratio of water to ethanol was low, the generated SiO_2 particles would continue to grow on the surface of hollow SiO_2 microspheres, which made the surface of the prepared microspheres relatively rough and caused the hollow microspheres to have a certain degree of agglomeration (Figure 3a). With the increase in water/ethanol, the surface of the microspheres became smoother (Figure 3b–d).

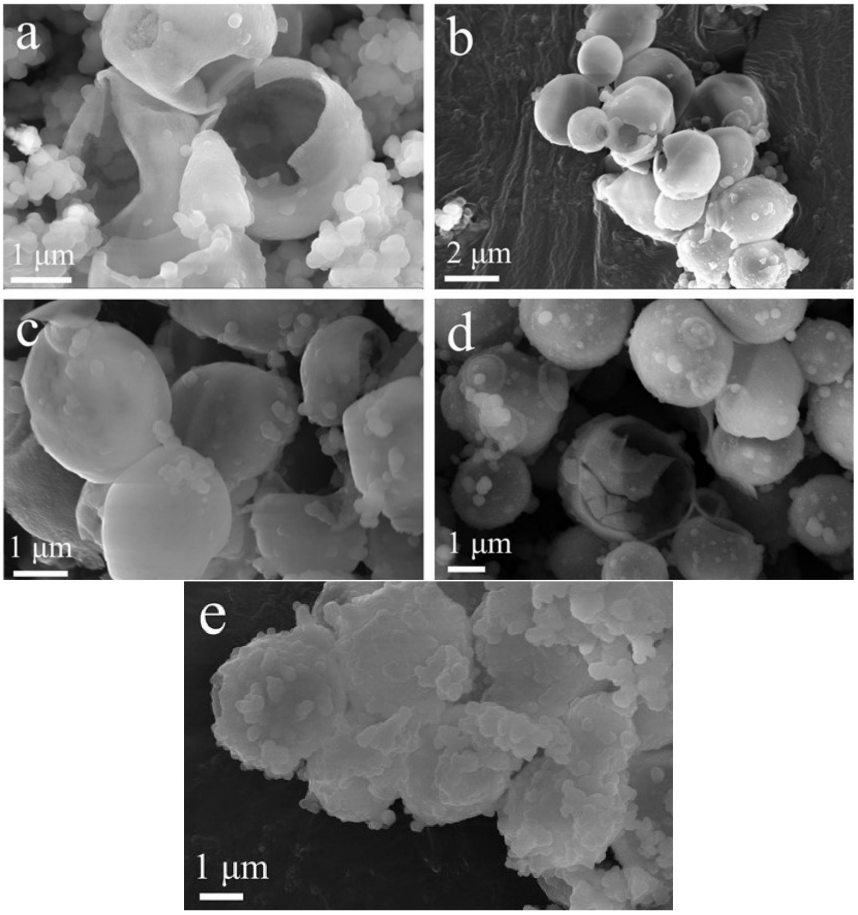

Figure 2. SEM images of SiO_2 synthesized at different TEOS concentrations: (**a**) 0.9 mol/L; (**b**) 1.0 mol/L; (**c**) 1.1 mol/L; (**d**) 1.2 mol/L; (**e**) 1.3 mol/L.

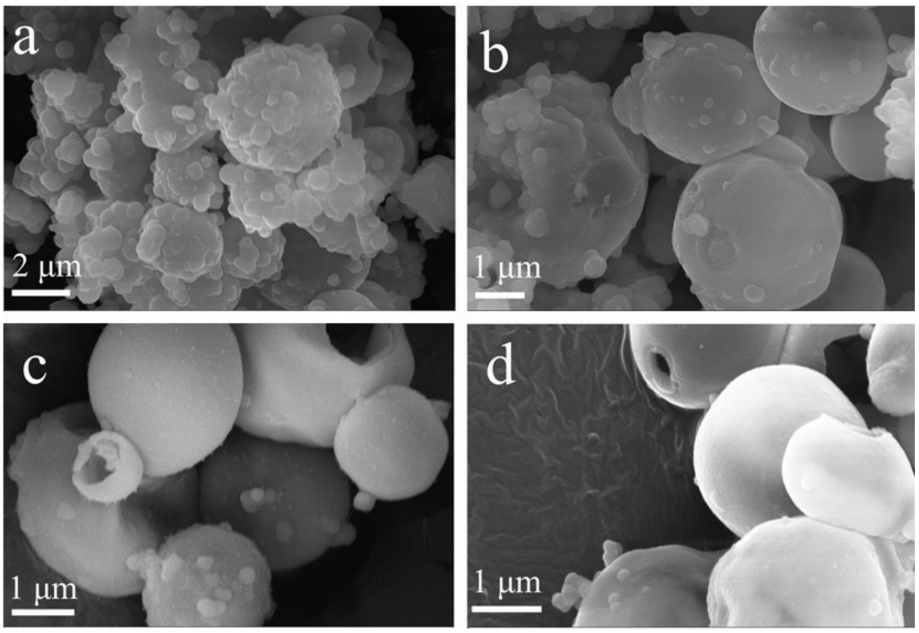

Figure 3. SEM images of SiO_2 synthesized at different ratios of water to ethanol: (**a**) 1/1; (**b**) 1/1.5; (**c**) 1/2; (**d**) 1/2.5.

3.1.4. Effect of Aging Time

The aging time also has an obvious effect on the surface of microspheres. As shown in Figure 4a, when the aging time was 6 h, the hollow SiO_2 microsphere structure was irregular and the dispersion was poor. With the aging time extended to 12 h, a complete hollow SiO_2 microsphere structure was formed with an even dispersion (Figure 4c). Complete hollow microsphere structures could be formed by extending the aging time (Figure 4d,e).

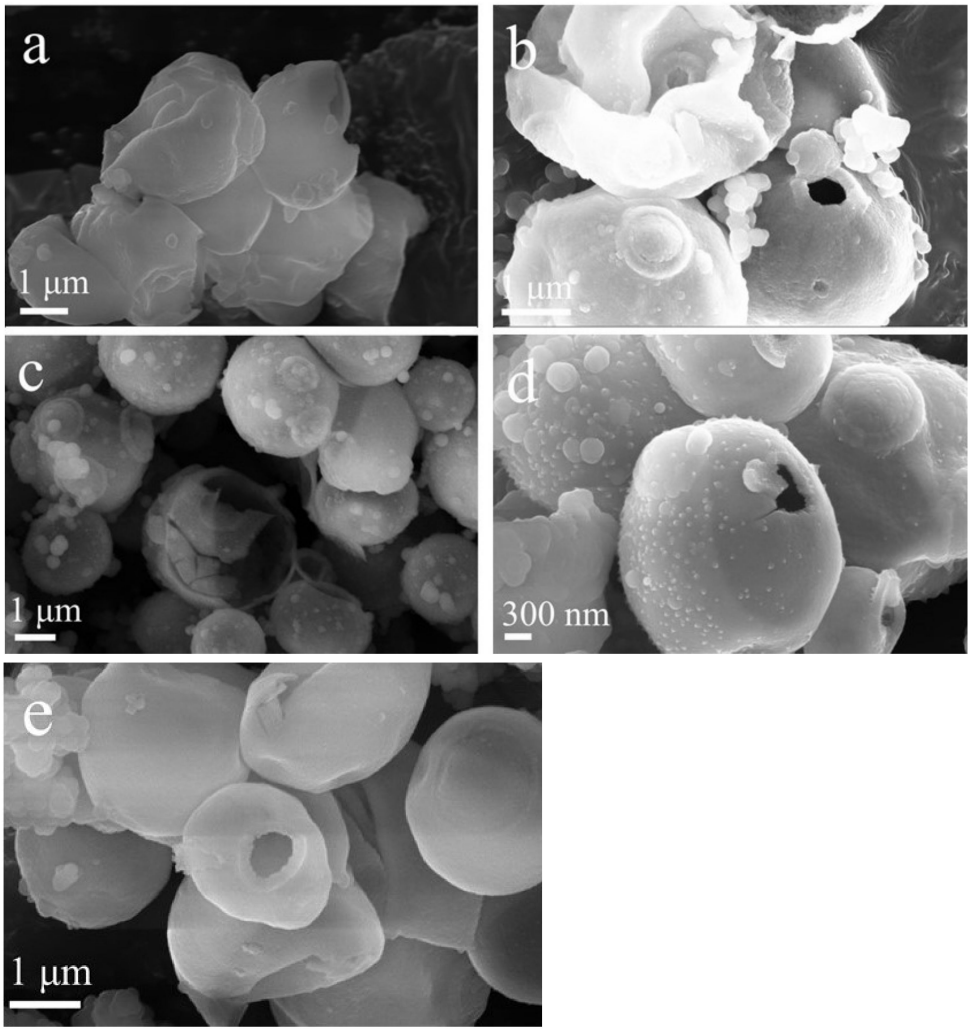

Figure 4. SEM images of SiO_2 synthesized at different aging times: (**a**) 6 h; (**b**) 10 h; (**c**) 12 h; (**d**) 24 h; (**e**) 36 h.

The TG and FTIR characterizations were performed and the results were shown in Figures A2 and A3. The results confirm the formation of SiO_2 and show that there may be some residual biomass on the microsphere.

3.2. Preparation of Hollow TiO_2-SiO_2

Based on the above, TiO_2 was coated on the surface of hollow SiO_2 microspheres to prepare TiO_2-SiO_2 by the hydrothermal method.

XRD patterns of SiO_2 and TiO_2-SiO_2 were displayed in Figure 5. The hollow SiO_2 microsphere was amorphous (curve a in Figure 5). The main peaks at 25.3°, 37.9°, 47.8°, 54.3°, and 63.0° in curve b could be assigned to the diffraction of the (101), (004), (200), (211), and (204) planes of anatase TiO_2 [36]. Generally, the anatase TiO_2 will change to rutile TiO_2 after high-temperature roasting. However, no rutile formation was found in this sample because of the spatial grid effect after silicon addition, which improved the

structural thermal stability of mesoporous TiO_2 and inhibited the transformation of anatase to rutile [37].

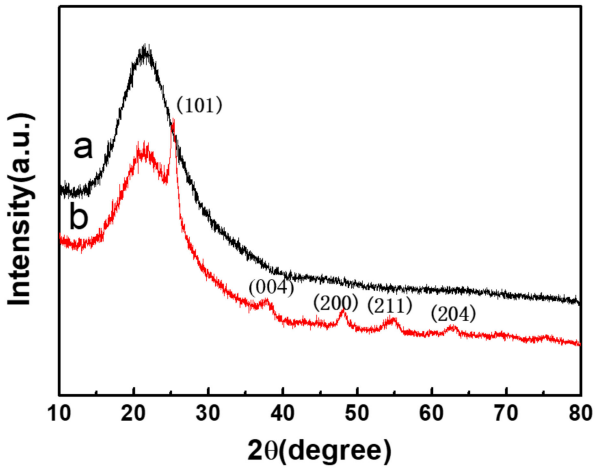

Figure 5. XRD patterns of SiO_2 and TiO_2-SiO_2.

To observe the microscopic morphology and internal structure of the prepared TiO_2-SiO_2, TEM characterization was carried out and the results were shown in Figure 6. In Figure 6a, a layer of material was successfully coated on the surface of SiO_2. The spacing of the lattice plane in Figure 6b was 0.35 nm, which was consistent with the d value of the (101) plane of the anatase TiO_2, confirming that the surfaces of the SiO_2 were successfully coated by TiO_2.

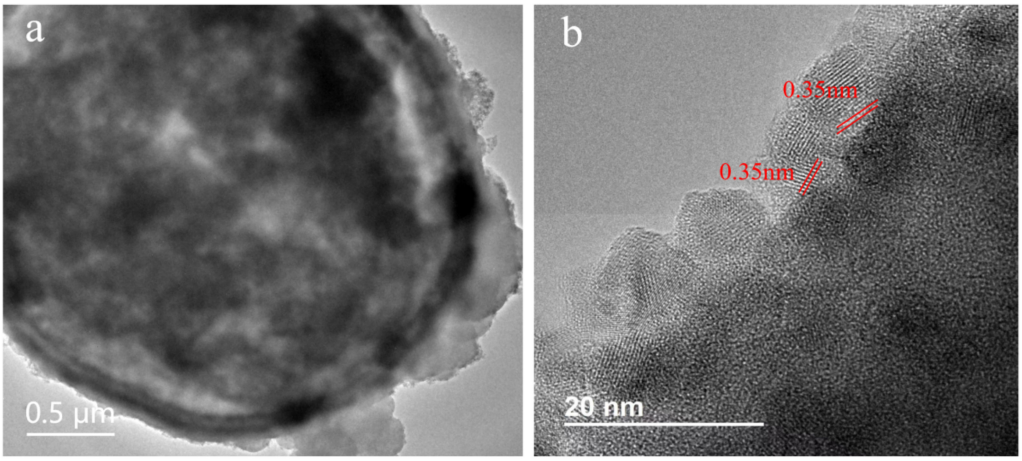

Figure 6. (**a**) TEM image and (**b**) high-resolution TEM image of the TiO_2-SiO_2.

In order to confirm the elemental composition and distribution of the TiO_2-SiO_2 catalyst, Si, O, and Ti elements were selected for an EDX surface scan. As shown in Figure 7, the distribution ranges of the O, Si, and Ti elements are consistent with the positions occupied by SiO_2 and the distribution is very uniform. This reflects not only the O and Si element properties of SiO_2, but also the fact that the titanium layer is successfully coated on the surface of the hollow SiO_2 microspheres.

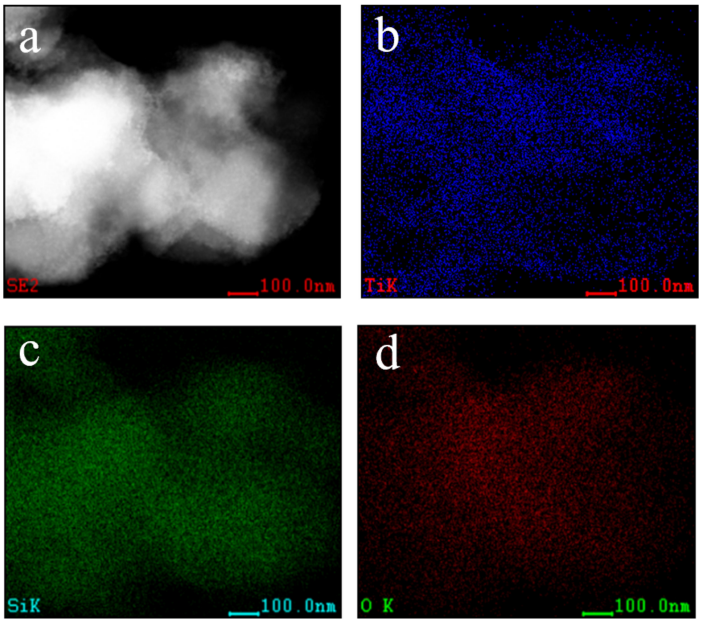

Figure 7. EDX elemental mapping investigation of (**a**) TiO_2-SiO_2 (**b**) Ti; (**c**) Si; (**d**) O.

The full XPS spectra of SiO_2 and TiO_2-SiO_2 were shown in Figure 8a and several peaks corresponding to Si, C, Ti, and O elements could be observed. Figure 8b showed the XPS spectrum of O1s of the sample SiO_2. The characteristic peak appeared at 532.3 eV and could be assigned to the binding energy of O 1s in Si-O-Si. The peak centered at around 103.3 eV in Figure 8c confirmed the presence of the Si element in SiO_2. A Ti 2p XPS spectrum of TiO_2-SiO_2 in Figure 8d was fitted into three peaks. The peaks located at 458.1 eV and 463.4 eV were assigned to Ti 2p3/2 and Ti 2p1/2 of TiO_2, respectively. A minor peak at 455.46 eV might be attributed to the low valence states of Ti [38]. The coating of TiO_2 exerted a great influence on the O 1s XPS spectrum (Figure 8e), which could be split into three peaks. The peak located at 529.6 eV and 532.7 eV were related to Ti–O–Ti and Si–O–Si. The peak at 532.0 eV could be assigned to the binding energy of the Si-O-Ti species, indicating the bonding of TiO_2 to SiO_2 [39]. Figure 8f showed the XPS spectrum of Si 2p of the sample TiO_2-SiO_2. There were two characteristic peaks of Si 2p located at 100.6 eV and 103.3 eV, showing that the coating of TiO_2 had an effect on the binding energy of the Si element.

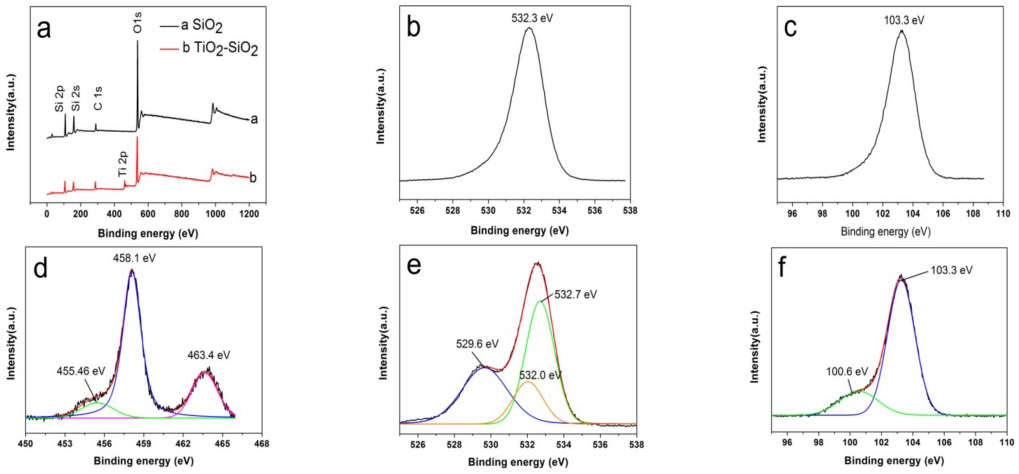

Figure 8. XPS spectra of SiO_2 and TiO_2-SiO_2. (**a**) Survey scan; (**b**) O 1s of SiO_2; (**c**) Si 2p of SiO_2; (**d**) Ti 2p of TiO_2-SiO_2; (**e**) O 1s of TiO_2-SiO_2; (**f**) Si 2p of TiO_2-SiO_2.

The specific surface area (S_{BET}), pore volume (V_P), and pore diameter (D_P) of different samples are summarized in Table 1. Compared with SiO_2 without a template, the specific surface area, pore volume, and pore diameter of SiO_2 produced by a yeast template increased by different degrees, and the increase in the specific surface area from 10.95 m^2 g^{-1} to 15.97 m^2 g^{-1} was mainly due to the successful formation of a hollow microsphere structure. When the hollow SiO_2 microspheres were coated with titanium, the specific surface area, pore volume, and pore diameter increased, which may be beneficial by providing more active sites and increasing the catalytic activity of the catalyst.

Table 1. Specific surface area and pore size distribution parameters of different samples.

Sample	S_{BET} (m^2g^{-1})	Vp (cm^3g^{-1})	Dp (nm)
SiO_2 without template	10.95	0.022	8.06
SiO_2 with yeast template	15.97	0.039	9.73
TiO_2-SiO_2	18.88	0.071	13.01

Figure 9a shows the N_2 adsorption–desorption isothermal curve and Barret Joyner Halenda (BJH) pore diameter distribution of SiO_2 prepared by the *P. pastoris* GS115 template. The N_2 adsorption–desorption isothermal curve belongs to the Langmuir-type IV mesoporous channel adsorption curve. At P/Po = 0.8–1.0, small hysteresis rings appears, which maybe have been caused by slight changes in the pore diameter of SiO_2 and the phenomenon of different pore sizes, and it could also have been caused by a small number of interstices between particles. The BJH pore diameter distribution diagram of SiO_2 inserted in Figure 9a shows that the mesopore diameter is in the range of 5 to 18 nm.

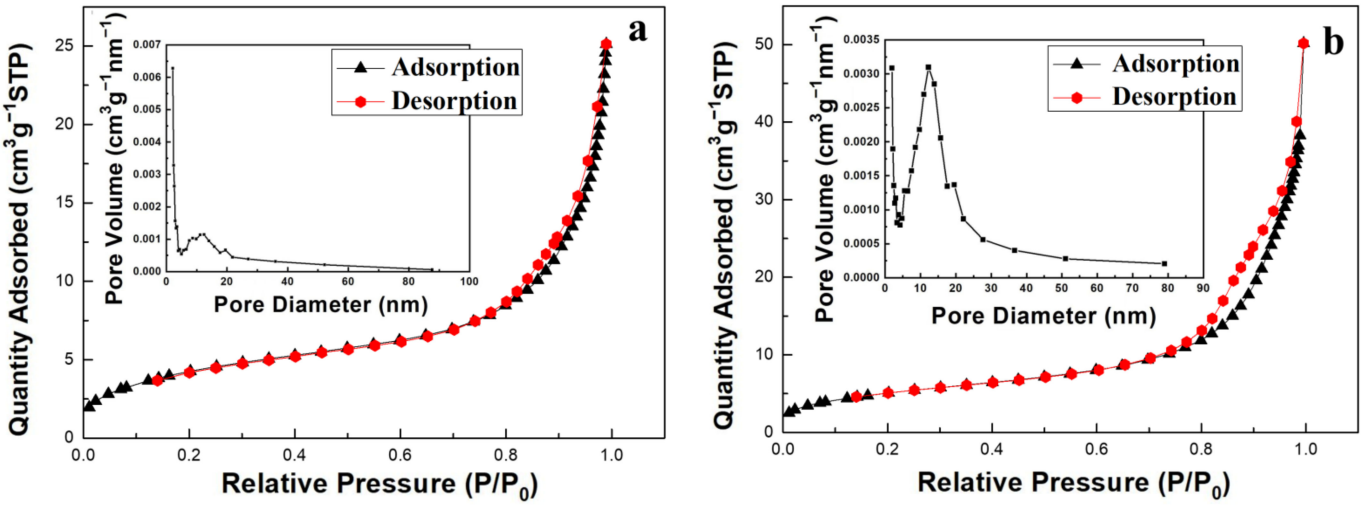

Figure 9. (**a**) N_2 adsorption–desorption isotherm curves of SiO_2. Inset is Barret Joyner Halenda (BJH) pore size distribution of SiO_2; (**b**) N_2 adsorption–desorption isotherm curves of TiO_2-SiO_2. Inset is BJH pore size distribution of TiO_2- SiO_2.

Figure 9b shows the N_2 adsorption–desorption isothermal curve and the BJH pore diameter distribution of TiO_2-SiO_2. At the low-pressure stage (P/Po < 0.8), there is a certain linear relationship between the adsorption amount and partial pressure, which may occur in a single layer of physical adsorption. When the partial pressure P/Po is approximately 0.8, the adsorption amount increases sharply and the adsorption enters the abrupt phase. The reason is that N_2 condenses the capillary in the mesoporous channel. When the partial pressure P/Po continues to increase, another abrupt jump occurs and a hysteresis ring appears under high partial pressure. At this time, N_2 condenses between material particles. It can be seen from the BJH pore diameter distribution curve inserted in Figure 9b that the sample pore diameter is mainly distributed between 5 and 20 nm. There are also concentrated holes, possibly caused by gaps between spherical particles of varying sizes.

3.3. Photocatalytic Activity

It could be seen from the Figure 10a that the absorbance of the solution was basically unchanged when the catalyst was not added. After the catalyst was introduced, the absorbance of MO gradually decreased with the extension of time. Moreover, the hollow TiO_2 microspheres were also prepared using *P. pastoris* GS115 as a template (see Figure A4). Comparing Figure 10b,c, it could be seen that the photocatalytic degradation ability of TiO_2-SiO_2 was higher than that of pure TiO_2 prepared with *P. pastoris* GS115 as a template. The probable cause was that the introduction of SiO_2 to TiO_2 could reduce its surface energy to a certain extent and reduce its agglomeration, forming active hydroxyl radicals, and thereby enhancing the photocatalytic ability of TiO_2 [40]. Jiang et al. [39] reported the preparation of hierarchical hollow TiO_2@SiO_2 composite microspherse and studied their photocatalytic performance on MO. The degradation rate was 99.7% after 3 h. Zhang et al. [41] prepared TiO_2/SiO_2 by the sol–gel method. The degradation rate of MO was 98.03% within 180 min using the 250 W mercury lamp as the light source. As shown in Figure 10c, the absorbance of MO was reduced to zero, indicating that MO was completely degraded in 100 min. The result suggests that the as-prepared TiO_2-SiO_2 microspheres exhibit an excellent photocatalytic activity.

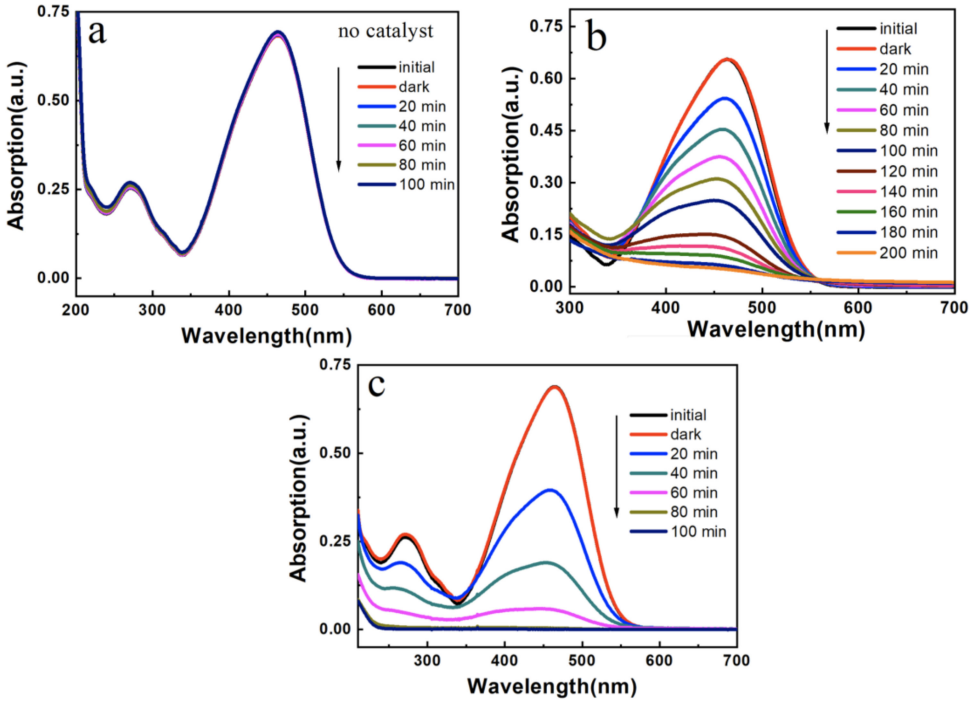

Figure 10. Photocatalytic activity of (**a**) no catalyst; (**b**) TiO_2 prepared from *P. pastoris* GS115 as a template; (**c**) TiO_2-SiO_2 prepared from *P. pastoris* GS115 as a template for MO degradation.

The estimated band gaps of pure TiO_2 and TiO_2-SiO_2 prepared with *P. pastoris* GS115 as a template are 3.23 eV and 3.63 eV, respectively (Figure 11). The band gap of TiO_2-SiO_2 is more than that of pure TiO_2, indicating that the introduction of silicon leads to an increase in the band gap of the semiconductor and enhances the redox capacity of holes and electrons. Hence, the photocatalytic activity can be improved.

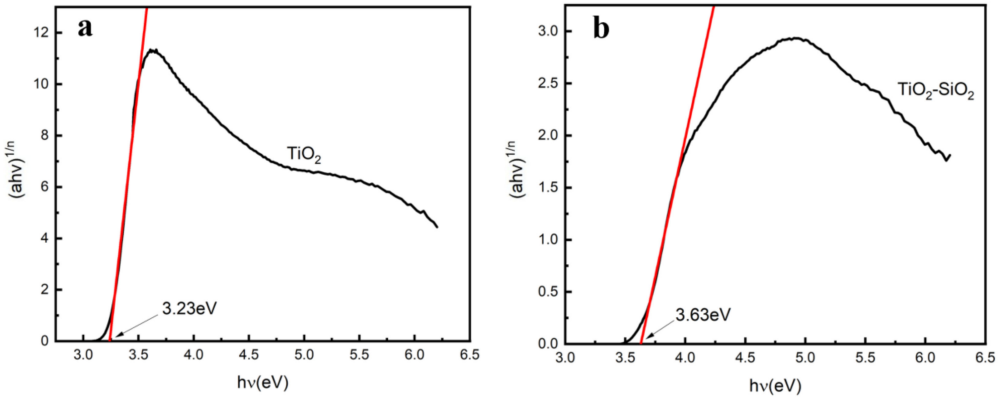

Figure 11. Estimated band gaps of (**a**) TiO_2 prepared from *P. pastoris* GS115 as a template and (**b**) TiO_2-SiO_2 prepared from *P. pastoris* GS115 as a template based on the Tauc/Davis–Mott model.

4. Conclusions

In summary, *P. pastoris* GS115 was employed as a typical microbe to demonstrate its potential in synthesizing high-efficient photocatalysts for the degradation of organic contaminants. Hollow SiO_2 microspheres with a spherical morphology were successfully synthesized using the microbe template. The morphology and surface roughness of the hollow particles could be controlled by the reaction conditions. TiO_2-SiO_2 microspheres were successfully prepared by the hydrothermal process. Results indicated that TiO_2-SiO_2 kept in the favorable anatase phase of TiO_2. The as-prepared TiO_2-SiO_2 exhibited good photocatalytic activity for the degradation of MO and the degradation rate could reach 99.9% in 100 min because of an increase in the band gap. This work is of great significance for employing microbes in the preparation of promising photocatalysts for large-scale practical application.

Author Contributions: Resources, X.J. and S.C.; Supervision, J.H. and Q.L.; Writing—original draft, S.L.; Writing—review & editing, L.L. All authors have read and agreed to the published version of the manuscript.

Funding: This research was funded by Natural Science Foundation of Fujian Province of China, grant number 2016J05044.

Institutional Review Board Statement: Not applicable.

Informed Consent Statement: Not applicable.

Data Availability Statement: The data presented in this study are available on request from the corresponding author.

Conflicts of Interest: The authors declare no conflict of interest.

Appendix A

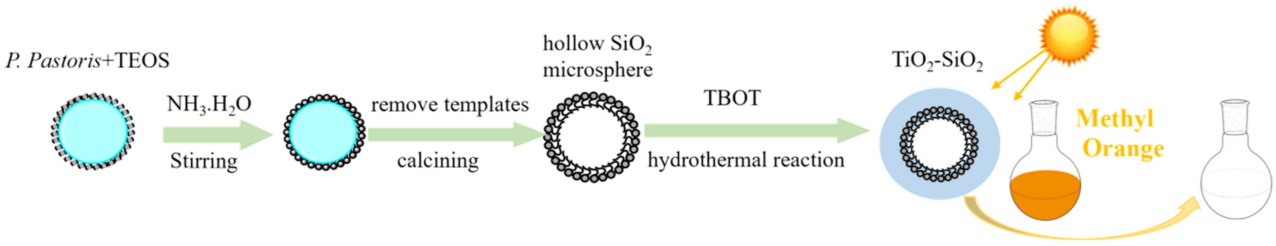

Figure A1. Reaction mechanism diagram.

When TEOS is added to a mixture of water and ethanol containing microorganism, TEOS is attached to the cell wall. After the addition of ammonia, TEOS begins to hydrolyze

and the resulting SiO_2 particles grow in the cell wall. Due to the slow hydrolysis rate of weak alkali in ammonia water, the adsorbed SiO_2 nanoparticles on the cell wall surface have enough time to grow. After calcination, the template is removed and the hollow SiO_2 microspheres are synthesized. TiO_2-SiO_2 microspheres are prepared by the hydrothermal process and the photocatalytic activity for the degradation of methyl orange (MO) at room temperature under Xe arc lamp acting as simulated sunlight was explored.

In order to investigate the influence of microbe templates on the preparation of SiO_2, the samples were characterized by TG. Figure A2 shows the TG characterization diagrams of *Pichia pastoris* GS115 and uncalcined SiO_2. From the TG spectrum of *P. pastoris* GS115, it can be seen that there is a small weight loss peak at 85 °C, which is mainly caused by the desorption of water on the surface of the sample; in the range of 200–700 °C, in the spectrum a distinct weight loss step appeared, which was caused by the gradual breakdown of the biomass molecules of the *P. pastoris* GS115. The TG spectrum of uncalcined SiO_2 microspheres is similar to the weight loss peak of *P. pastoris* GS115, which indicates that some biomass may remain on the surface of the uncalcined SiO_2 microspheres.

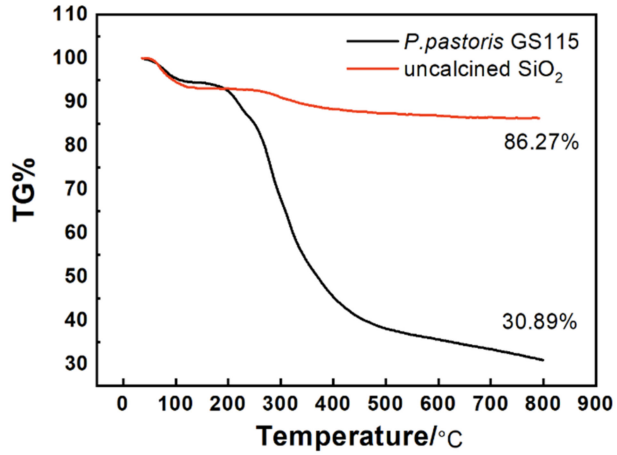

Figure A2. TG curves of *P. pastoris* GS115 and uncalcined SiO_2 (conditions: TEOS concentration 1.2 mol/L, the ratio of water to ethanol 1/2, aging time 12 h).

From the spectrum of uncalcined SiO_2 in Figure A3, the structural water –OH anti scaling vibration peak appears at 3450 cm^{-1}, and the peak near 1638cm^{-1} is the H–OH bend vibration peak of water. The peak at 955 cm^{-1} belongs to the bending vibration absorption peak of Si–OH, which is consistent with the literature reports. After calcination, the strong and wide absorption band at 1095 cm^{-1} is attributed to Si–O–Si anti scaling vibration peak, and the peak at 798cm^{-1} is attributed to Si–O symmetric stretching vibration peak.

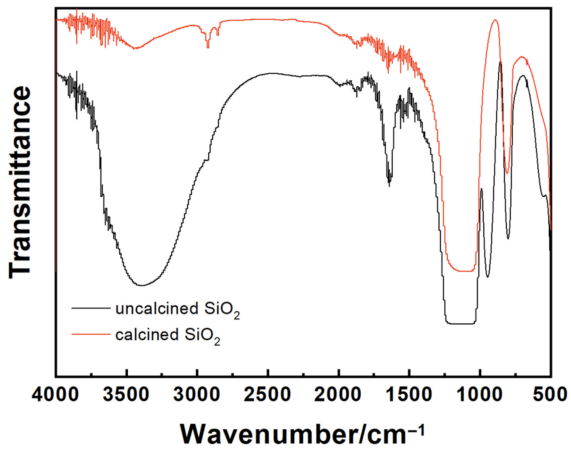

Figure A3. FT-IR spectra of SiO_2.

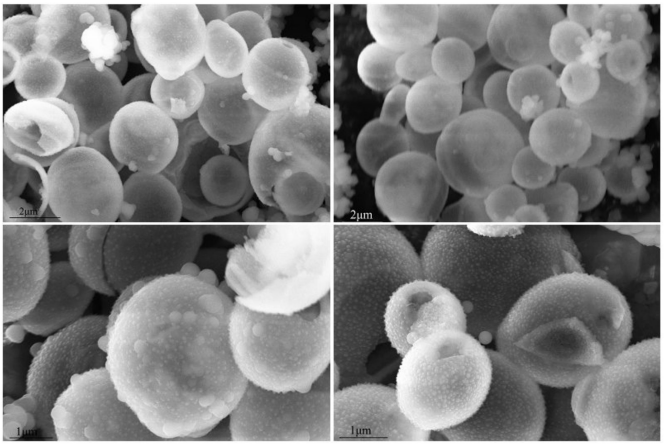

Figure A4. SEM images of TiO_2 prepared from *P. pastoris* GS115 as a template.

References

1. Behera, M.; Nayak, J.; Banerjee, S.; Chakrabortty, S.; Tripathy, S.K. A review on the treatment of textile industry waste effluents towards the development of efficient mitigation strategy: An integrated system design approach. *J. Environ. Chem. Eng.* **2021**, *9*, 105277. [CrossRef]
2. Kishor, R.; Purchase, D.; Saratale, G.D.; Saratale, R.G.; Ferreira, L.F.R.; Bilal, M.; Chandra, R.; Bharagava, R.N. Ecotoxicological and health concerns of persistent coloring pollutants of textile industry wastewater and treatment approaches for environmental safety. *J. Environ. Chem. Eng.* **2021**, *9*, 105012. [CrossRef]
3. Konicki, W.; Aleksandrzak, M.; Moszyński, D.; Mijowska, E. Adsorption of anionic azo-dyes from aqueous solutions onto graphene oxide: Equilibrium, kinetic and thermodynamic studies. *J. Colloid Interface Sci.* **2017**, *496*, 188–200. [CrossRef] [PubMed]
4. Tran, T.H.; Le, H.H.; Pham, T.H.; Nguyen, D.T.; La, D.D.; Chang, S.W.; Lee, S.M.; Chung, W.J. Comparative study on methylene blue adsorption behavior of coffee husk-derived activated carbon materials prepared using hydrothermal and soaking methods. *J. Environ. Chem. Eng.* **2021**, *9*, 105362. [CrossRef]
5. Domenzain-Gonzalez, J.; Castro-Arellano, J.J.; Galicia-Luna, L.A.; Rodriguez-Cruz, M.; Hernandez-Lopez, R.T.; Lartundo-Rojas, L. Photocatalytic membrane reactor based on Mexican Natural Zeolite: RB5 dye removal by photo-Fenton process. *J. Environ. Chem. Eng.* **2021**, *9*, 105281. [CrossRef]
6. Verma, P.; Samanta, S.K.; Mishra, S. Photon-independent NaOH/H_2O_2–based degradation of rhodamine-B dye in aqueous medium: Kinetics, and impacts of various inorganic salts, antioxidants, and urea. *J. Environ. Chem. Eng.* **2020**, *8*, 103851. [CrossRef]
7. Arslan-Alaton, I.; Tureli, G.; Olmez-Hanci, T. Treatment of azo dye production wastewaters using Photo-Fenton-like advanced oxidation processes: Optimization by response surface methodology. *J. Photochem. Photobiol. A Chem.* **2009**, *202*, 142–153. [CrossRef]
8. Muruganandham, M.; Swaminathan, M. Photochemical oxidation of reactive azo dye with UV–H_2O_2 process. *Dyes Pigments* **2004**, *62*, 269–275. [CrossRef]
9. Neamtu, M.; Siminiceanu, I.; Yediler, A.; Kettrup, A. Kinetics of decolorization and mineralization of reactive azo dyes in aqueous solution by the UV/H_2O_2 oxidation. *Dyes Pigments* **2002**, *53*, 93–99. [CrossRef]
10. Dang, T.-D.; Nguyen-Thi, L.; Nguyen-Xuan, T.; Le, H.T.; Vo, H.T.; Nguyen, T.H.P.; La, D.D.; Kim, G.-M.; Chang, S.W.; Nguyen, D.D. Hierarchical zero-valent iron fabricated from microfluidic reactor for the removal of organic dyes from aqueous media. *Sustain. Energy Technol. Assess.* **2021**, *44*, 101031. [CrossRef]
11. La, D.D.; Jadha, R.W.; Gosavi, N.M.; Rene, E.R.; Nguyen, T.A.; Xuan-Thanh, B.; Nguyen, D.D.; Chung, W.J.; Chang, S.W.; Nguyen, X.H.; et al. Natureinspired organic semiconductor via solvophobic self-assembly of porphyrin derivative as an effective photocatalyst for degradation of rhodamine B dye. *J. Water Process Eng.* **2021**, *40*, 101876. [CrossRef]
12. Ahila, K.G.; Ravindran, B.; Muthunarayanan, V.; Nguyen, D.D.; Nguyen, X.C.; Chang, S.W.; Nguyen, V.K.; Thamaraiselvi, C. Phytoremediation potential of freshwater macrophytes for treating dye-containing wastewater. *Sustainability* **2021**, *13*, 329. [CrossRef]
13. Türgay, O.; Ersoz, G.; Atalay, S.; Forss, J.; Welander, U. The treatment of azo dyes found in textile industry wastewater by anaerobic biological method and chemical oxidation. *Sep. Purif. Technol.* **2011**, *79*, 26–33. [CrossRef]
14. Chaturvedi, A.; Rai, B.N.; Singh, R.S.; Jaiswal, R.P. Comparative toxicity assessment using plant and luminescent bacterial assays after anaerobic treatments of dyeing wastewater in a recirculating fixed bed bioreactor. *J. Environ. Chem. Eng.* **2021**, *9*, 105466. [CrossRef]
15. Jangid, N.K.; Jadoun, S.; Yadav, A.; Srivastava, M.; Kaur, N. Polyaniline-TiO_2-based photocatalysts for dyes degradation. *Polym. Bull.* **2021**, *78*, 4743–4777. [CrossRef]

16. Fernández-Pérez, A.; Marbán, G. Titanium dioxide: A heterogeneous catalyst for dark peroxidation superior to iron oxide. *J. Environ. Chem. Eng.* **2020**, *8*, 104254. [CrossRef]
17. Thi-Tuyet Hoang, M.; Thi-Kim Tran, A.; Suc, N.V. The-Vinh Nguyen, Antibacterial activities of gel-derived Ag-TiO_2-SiO_2 nanomaterials under different light irradiation. *AIMS Mater. Sci.* **2015**, *3*, 339–348. [CrossRef]
18. Wanag, A.; Sienkiewicz, A.; Rokicka-Konieczna, P.; Kusiak-Nejman, E.; Morawski, A.W. Influence of modification of titanium dioxide by silane coupling agents on the photocatalytic activity and stability. *J. Environ. Chem. Eng.* **2020**, *8*, 103917. [CrossRef]
19. Lakshmanareddy, N.; Rao, V.N.; Cheralathan, K.K.; Subramaniam, E.P.; Shankar, M.V. Pt/TiO_2 nanotube photocatalyst—Effect of synthesis methods on valance state of Pt and its influence on hydrogen production and dye degradation. *J. Colloid Interf. Sci.* **2019**, *538*, 83–98. [CrossRef]
20. Wang, J.D.; Gu, Z.J.; Zhang, J.L.; Chen, X.; Li, M.J.; Yu, Y.; Ge, M.Q.; Li, X.Q. Mesoporous structure TiO_2/SiO_2 composite for methylene blue adsorption and photodegradation. *Micro. Nano. Lett.* **2019**, *14*, 323–328. [CrossRef]
21. Saroj, S.; Singh, L.; Singh, S.V. Photodegradation of direct blue-199 in carpet industry wastewater using iron-doped TiO_2 nanoparticles and regenerated photocatalyst. *Int. J. Chem. Kinet.* **2019**, *51*, 189–205. [CrossRef]
22. Zhang, W.P.; Li, G.Y.; Liu, H.L.; Chen, J.Y.; Ma, S.T.; An, T.C. Micro/nano-bubble assisted synthesis of Au/TiO2@CNTs composite photocatalyst for photocatalytic degradation of gaseous styrene and its enhanced catalytic mechanism. *Environ. Sci-Nano* **2019**, *6*, 948–958. [CrossRef]
23. Huang, J.J.; Jing, H.X.; Li, N.; Jiao, L.X.; Zhou, W. Fabrication of magnetically recyclable SnO_2-TiO_2/$CoFe_2O_4$ hollow core-shell photocatalyst: Improving photocatalytic efficiency under visible light irradiation. *J. Solid State Chem.* **2019**, *271*, 103–109. [CrossRef]
24. Smeets, V.; Boissiere, C.; Sanchez, C.; Gaigneaux, E.M.; Peeters, E.; Sels, B.F.; Dusselier, M.; Debecker, D.P. Aerosol route to TiO_2-SiO_2 catalysts with tailored pore architecture and high epoxidation activity. *Chem. Mater.* **2019**, *31*, 1610–1619. [CrossRef]
25. Wang, W.; Chen, H.; Fang, J.; Lai, M. Large-scale preparation of rice-husk-derived mesoporous SiO_2@TiO_2 as efficient and promising photocatalysts for organic contaminants degradation. *App. Surf. Sci.* **2019**, *467*, 1187–1194. [CrossRef]
26. Wu, Y.; Li, M.; Yuan, J.; Lu, J.; Wu, P.; Liu, C.; Wang, X. Rapid preparation of TiO_2-SiO_2 heterostructure photonic crystal in the near infrared region via a modified electrophoresis-assisted self-assembly process. *Mater. Res. Bull.* **2018**, *100*, 353–356. [CrossRef]
27. Wu, J.; He, X.D.; Li, G.Z.; Deng, J.H.; Chen, L.; Xue, W.B.; Li, D.J. Rapid construction of TiO_2/SiO_2 composite film on Ti foil as lithium-ion battery anode by plasma discharge in solution. *Appl. Phys. Lett.* **2019**, *114*, 043903–043908. [CrossRef]
28. Zhou, Z.R.; Dong, P.; Wang, D.Y.; Liu, M.; Duan, J.G.; Nayaka, G.P.; Wang, D.; Xu, C.Y.; Hua, Y.X.; Zhang, Y.J. Silicon-titanium nanocomposite synthesized via the direct electrolysis of SiO_2/TiO_2 precursor in molten salt and their performance as the anode material for lithium-ion batteries. *J. Alloy Compd.* **2019**, *781*, 362–370. [CrossRef]
29. Hao, N.; Nie, Y.; Xu, Z.; Closson, A.B.; Usherwood, T.; Zhang, J.X. Microfluidic continuous flow synthesis of functional hollow spherical silica with hierarchical sponge-like large porous shell. *Chem. Eng. J.* **2019**, *366*, 433–438. [CrossRef]
30. He, J.Q.; Chen, D.Y.; Li, N.J.; Xu, Q.F.; Li, H.; He, J.H.; Lu, J.M. Hollow mesoporous Co_3O_4-CeO_2 composite nanotubes with open ends for efficient catalytic CO oxidation. *J. ChemSusChem* **2019**, *12*, 1084–1090. [CrossRef]
31. Tardy, B.L.; Richardson, J.J.; Guo, J.; Lehtonen, J.; Ago, M.; Rojas, O.J. Lignin nano- and microparticles as template for nanostructured materials: Formation of hollow metal-phenolic capsules. *Green Chem.* **2018**, *20*, 1335–1344. [CrossRef]
32. Atla, S.B.; Chen, Y.-J.; Chiu, H.-W.; Chen, C.-C.; Shu, J.-C. Microbial induced synthesis of $CeCO_3OH$ and CeO_2 hollow rods micro/nanostructure. *Mater. Lett.* **2016**, *167*, 238–241. [CrossRef]
33. Wei, L.; Ma, M.X.; Lu, Y.H.; Wang, D.S.; Zhang, S.L.; Zhao, T.; Ma, W.P. Hydrogen generation from hydrolysis of sodium borohydride using Co_3O_4 hollow microspheres synthesized with yeast template. *J. Inorg. Mater.* **2018**, *33*, 648–652.
34. Tripathi, R.; Narayan, A.; Bramhecha, I.; Sheikh, J. Development of multifunctional linen fabric using chitosan film as a template for immobilization of in-situ generated CeO_2 nanoparticles. *Int. J. Biol. Macromol.* **2019**, *121*, 1154–1159. [CrossRef]
35. Records, W.C.; Yoon, Y.; Ohmura, J.; Chanut, N.; Belcher, A.M. Virus-templated Pt-Ni$(OH)_2$ nanonetworks for enhanced electrocatalytic reduction of water. *Nano Energy* **2019**, *58*, 167–174. [CrossRef]
36. Yaacob, K.A.; Riley, J.D. Study on the influence of synthesis temperature of anatase TiO_2 nanoparticles for electrophoretic deposition. *Adv. Mater. Res.* **2013**, *620*, 161–165. [CrossRef]
37. Jongsomjit, B.; Wongsalee, T.; Praserthdam, P. Catalytic behaviors of mixed TiO_2-SiO_2-supported cobalt Fischer–Tropsch catalysts for carbon monoxide hydrogenation. *Mater. Chem. Phys.* **2006**, *97*, 343–350. [CrossRef]
38. Esfandiaria, N.; Kashefia, M.; Mirjalilia, M.; Afsharnezhad, S. Role of silica mid-layer in thermal and chemical stability of hierarchical Fe_3O_4-SiO_2-TiO_2 nanoparticles for improvement of lead adsorption: Kinetics, thermodynamic and deep XPS investigation. *Mat. Sci. Eng. B* **2020**, *262*, 114690. [CrossRef]
39. Jiang, Q.; Huang, J.; Ma, B.; Yang, Z.; Zhang, T.; Wang, X. Recyclable, hierarchical hollow photocatalyst TiO_2@SiO_2 composite microsphere realized by raspberry-like SiO_2. *Colloid Surface A* **2020**, *602*, 125112. [CrossRef]
40. Deng, H.; Jiang, X. Preparation of TiO_2/SiO_2 and photocatalytic degradation of Methyl Orange. *J. Textile* **2007**, *28*, 76–83.
41. Zhang, C.H.; Li, J.; Chen, Z.M.; Zhu, Q.F. Preparation of TiO_2/SiO_2 and photocatalytic oxidative degradation of methyl orange. *J. North Cent. Univ.* **2015**, *36*, 682–688.